

Optical properties of silicon germanium waveguides at telecommunication wavelengths

Kamal Hammani,^{1,*} Mohamed A. Ettabib,¹ Adonis Bogris,^{2,3} Alexandros Kapsalis,²
Dimitris Syvridis,² Mickael Brun,⁴ Pierre Labeye,⁴ Sergio Nicoletti,⁴
David J. Richardson,¹ and Periklis Petropoulos¹

¹Optoelectronics Research Centre, University of Southampton, Highfield, Southampton, SO17 1BJ, UK

²National and Kapodistrian University of Athens, Panepistimiopolis, Ilissia, 15784, Athens, Greece

³Department of Informatics, Technological Educational Institute of Athens, Aghiou Spiridonos, 12210 Egaleo, Athens, Greece

⁴CEA-Leti MINATEC Campus, 17 rue des Martyrs 38054 Grenoble Cedex 9, France

*K.Hammani@soton.ac.uk

Abstract: We present a systematic experimental study of the linear and nonlinear optical properties of silicon-germanium (SiGe) waveguides, conducted on samples of varying cross-sectional dimensions and Ge concentrations. The evolution of the various optical properties for waveguide widths in the range 0.3 to 2 μm and Ge concentrations varying between 10 and 30% is considered. Finally, we comment on the comparative performance of the waveguides, when they are considered for nonlinear applications at telecommunication wavelengths.

©2013 Optical Society of America

OCIS codes: (130.3120) Integrated optics devices; (160.4760) Optical properties; (190.4390) Nonlinear optics, integrated optics; (230.7390) Waveguides, planar.

References and links

1. J. Leuthold, C. Koos, and W. Freude, "Nonlinear silicon photonics," *Nat. Photonics* **4**(8), 535–544 (2010).
2. O. Boyraz, T. Indukuri, and B. Jalali, "Self-phase-modulation induced spectral broadening in silicon waveguides," *Opt. Express* **12**(5), 829–834 (2004).
3. E. Dulkeith, Y. A. Vlasov, X. G. Chen, N. C. Panoiu, and R. M. Osgood, Jr., "Self-phase-modulation in submicron silicon-on-insulator photonic wires," *Opt. Express* **14**(12), 5524–5534 (2006).
4. H. K. Tsang, C. S. Wong, T. K. Liang, I. E. Day, S. W. Roberts, A. Harpin, J. Drake, and M. Asghari, "Optical dispersion, two-photon absorption and self-phase modulation in silicon waveguides at 1.5 μm wavelength," *Appl. Phys. Lett.* **80**(3), 416–418 (2002).
5. H. Fukuda, K. Yamada, T. Shoji, M. Takahashi, T. Tsuchizawa, T. Watanabe, J. Takahashi, and S. Itabashi, "Four-wave mixing in silicon wire waveguides," *Opt. Express* **13**(12), 4629–4637 (2005).
6. M. A. Foster, A. C. Turner, J. E. Sharping, B. S. Schmidt, M. Lipson, and A. L. Gaeta, "Broad-band optical parametric gain on a silicon photonic chip," *Nature* **441**(7096), 960–963 (2006).
7. R. Claps, D. Dimitropoulos, Y. Han, and B. Jalali, "Observation of Raman emission in silicon waveguides at 1.54 μm ," *Opt. Express* **10**(22), 1305–1313 (2002).
8. O. Boyraz and B. Jalali, "Demonstration of a silicon Raman laser," *Opt. Express* **12**(21), 5269–5273 (2004).
9. H. S. Rong, A. S. Liu, R. Jones, O. Cohen, D. Hak, R. Nicolaescu, A. Fang, and M. Paniccia, "An all-silicon Raman laser," *Nature* **433**(7023), 292–294 (2005).
10. H. K. Tsang and Y. Liu, "Nonlinear optical properties of silicon waveguides," *Semicond. Sci. Technol.* **23**(6), 064007 (2008).
11. J. P. Douglas, "Si/SiGe heterostructures: from material and physics to devices and circuits," *Semicond. Sci. Technol.* **19**(10), R75–R108 (2004).
12. P. Chaisakul, D. Marris-Morini, M.-S. Rouified, G. Isella, D. Chrastina, J. Frigerio, X. Le Roux, S. Edmond, J.-R. Coudevylle, and L. Vivien, "23 GHz Ge/SiGe multiple quantum well electro-absorption modulator," *Opt. Express* **20**(3), 3219–3224 (2012).
13. L. Tsybeskov and D. J. Lockwood, "Silicon-Germanium nanostructures for light emitters and on-chip optical interconnects," *Proc. IEEE* **97**(7), 1284–1303 (2009).
14. P. Chaisakul, D. Marris-Morini, G. Isella, D. Chrastina, M. S. Rouified, X. Le Roux, S. Edmond, E. Cassan, J. R. Coudevylle, and L. Vivien, "10-Gb/s Ge/SiGe multiple quantum-well waveguide photodetector," *IEEE Photon. Technol. Lett.* **23**(20), 1430–1432 (2011).
15. N. K. Hon, R. Soref, and B. Jalali, "The third-order nonlinear optical coefficients of Si, Ge, and Si1-xGex in the midwave and longwave infrared," *J. Appl. Phys.* **110**(1), 011301 (2011).
16. Q. Lin, T. J. Johnson, R. Perahia, C. P. Michael, and O. J. Painter, "A proposal for highly tunable optical parametric oscillation in silicon micro-resonators," *Opt. Express* **16**(14), 10596–10610 (2008).

17. J. Humlíček, A. Röseler, T. Zettler, M. G. Kekoua, and E. V. Khoutishvili, "Infrared refractive index of germanium-silicon alloy crystals," *Appl. Opt.* **31**(1), 90–94 (1992).
18. H. García and R. Kalyanaraman, "Phonon-assisted two-photon absorption in the presence of a dc-field: the nonlinear Franz–Keldysh effect in indirect gap semiconductors," *J. Phys. At. Mol. Opt. Phys.* **39**(12), 2737–2746 (2006).
19. Q. Lin, O. J. Painter, and G. P. Agrawal, "Nonlinear optical phenomena in silicon waveguides: modeling and applications," *Opt. Express* **15**(25), 16604–16644 (2007).
20. G. Tittelbach, B. Richter, and W. Karthe, "Comparison of three transmission methods for integrated optical waveguide propagation loss measurement," *Pure Appl. Opt.* **2**(6), 683–700 (1993).
21. H. K. Tsang, R. V. Penty, I. H. White, R. S. Grant, W. Sibbett, J. B. D. Soole, H. P. LeBlanc, N. C. Andreadakis, R. Bhat, and M. A. Koza, "Two-photon absorption and self-phase modulation in InGaAsP/InP multi-quantum-well waveguides," *J. Appl. Phys.* **70**(7), 3992–3994 (1991).
22. T. K. Liang and H. K. Tsang, "Nonlinear absorption and Raman scattering in silicon-on-insulator optical waveguides," *IEEE J. Sel. Top. Quantum Electron.* **10**(5), 1149–1153 (2004).
23. A. D. Bristow, N. Rotenberg, and H. M. van Driel, "Two-photon absorption and Kerr coefficients of silicon for 850–2200 nm," *Appl. Phys. Lett.* **90**(19), 191104 (2007).
24. A. Boskovic, S. V. Chernikov, J. R. Taylor, L. Gruner-Nielsen, and O. A. Levring, "Direct continuous-wave measurement of n_2 in various types of telecommunication fiber at 1.55 μm ," *Opt. Lett.* **21**(24), 1966–1968 (1996).
25. A. Lamminpää, T. Niemi, E. Ikonen, P. Marttila, and H. Ludvigsen, "Effects of dispersion on nonlinearity measurement of optical fibers," *Opt. Fiber Technol.* **11**(3), 278–285 (2005).
26. E. Dulkeith, F. N. Xia, L. Schares, W. M. J. Green, and Y. A. Vlasov, "Group index and group velocity dispersion in silicon-on-insulator photonic wires," *Opt. Express* **14**(9), 3853–3863 (2006).
27. S. Mas, J. Matres, J. Marti, and C. J. Oton, "Accurate chromatic dispersion characterization of photonic integrated circuits," *IEEE Photon. J.* **4**(3), 825–831 (2012).
28. B. Batagelj, "Conversion efficiency of fiber wavelength converter based on degenerate FWM," in *2nd International Conference on Transparent Optical Networks (ICTON)*, (2000), pp. 179–182.
29. N. Shibata, R. Braun, and R. Waarts, "Phase-mismatch dependence of efficiency of wave generation through four-wave mixing in a single-mode optical fiber," *IEEE J. Quantum Electron.* **23**(7), 1205–1210 (1987).
30. T. Vallaitis, S. Bogatscher, L. Alloatti, P. Dumon, R. Baets, M. L. Scimeca, I. Biaggio, F. Diederich, C. Koos, W. Freude, and J. Leuthold, "Optical properties of highly nonlinear silicon-organic hybrid (SOH) waveguide geometries," *Opt. Express* **17**(20), 17357–17368 (2009).
31. K. W. DeLong, K. B. Rochford, and G. I. Stegeman, "Effect of two-photon absorption on all-optical guided-wave devices," *Appl. Phys. Lett.* **55**(18), 1823–1825 (1989).
32. V. Mizrahi, K. W. DeLong, G. I. Stegeman, M. A. Saifi, and M. J. Andrejco, "Two-photon absorption as a limitation to all-optical switching," *Opt. Lett.* **14**(20), 1140–1142 (1989).
33. M. A. Ettabib, K. Hammani, F. Parmigiani, L. Jones, A. Kapsalis, A. Bogris, D. Syvridis, M. Brun, P. Labeye, S. Nicoletti, and P. Petropoulos, "FWM-based wavelength conversion in a silicon germanium waveguide," in *OFC/NFOEC* (Anaheim, CA, USA, 2013), p. OTh1C.4.
34. M. A. Ettabib, K. Hammani, F. Parmigiani, L. Jones, A. Kapsalis, A. Bogris, D. Syvridis, M. Brun, P. Labeye, S. Nicoletti, and P. Petropoulos, "FWM-based wavelength conversion of 40 Gbaud PSK signals in a silicon germanium waveguide," *Opt. Express* (to be published).

1. Introduction

Silicon photonics has attracted considerable attention as an emerging technology for all-optical processing in recent years, owing mainly to the attraction of silicon as a nonlinear material [1]. The large Kerr nonlinear coefficient ($n_2 = 4.5 \times 10^{-18} \text{ m}^2 \cdot \text{W}^{-1}$) and strongly confined modes have allowed the demonstration of self-phase modulation [2–4], four wave mixing [5] and associated parametric amplification [6], as well as stimulated Raman scattering [7] and its application for the implementation of Raman lasers [8, 9]. Although such great results are possible thanks to the good optical properties of silicon waveguides [10], a mix of silicon (Si) with other elements, and in particular germanium (Ge), can strongly enhance the nonlinear response.

The silicon-germanium (SiGe) alloy has emerged as an attractive material for both micro- and opto-electronic devices thanks to the potential for band gap and lattice parameter engineering that it offers [11]. For instance, SiGe modulators [12], light emitters [13] and photodetectors [14] have already been demonstrated. Very recently, SiGe alloys have also been identified as promising candidates for nonlinear applications in the midwave and longwave infrared exhibiting stronger nonlinearities, as compared to pure Si [15]. Of course, the nonlinear properties of SiGe waveguides could also be interesting in the near-infrared and particularly at optical communication wavelengths. However, though germanium enhances

the nonlinear response, this comes at the expense of an increase in the propagation loss due to the absorptive properties of Ge.

In this paper, we investigate the potential use of $\text{Si}_{1-x}\text{Ge}_x$ waveguides for nonlinear applications at telecommunication wavelengths. Waveguides of various widths and with a varying concentration in Ge have been fabricated in order to carry out a systematic study of their linear and nonlinear optical properties. The experimental analysis shows that the waveguide losses vary from 0.5 dB/cm to more than 5 dB/cm as the fractional Ge concentration increases from 0.1 to 0.3. On the other hand, the nonlinearity is also enhanced, increasing from less than $10 \text{ W}^{-1}\cdot\text{m}^{-1}$ to almost $40 \text{ W}^{-1}\cdot\text{m}^{-1}$. The impact of two-photon absorption (TPA) is discussed as well as the evolution of the four-wave mixing (FWM) bandwidth. Finally, we compare the overall performance of the different waveguides and perform a tradeoff analysis. Our experimental results are supported by numerical modeling showing satisfactory agreement.

2. Fabrication and structure of waveguides

The devices consisted of epi-layers of SiGe grown on a Si substrate. First, $1.4 \mu\text{m}$ thick SiGe layers with different germanium concentrations were grown by reduced pressure chemical vapor deposition (RP-CVD) to control the Ge concentration in great precision and thus preserve uniformity. Standard photolithography and deep reactive ion etching techniques were used to form the strips. Finally, the waveguides were encapsulated with a $12 \mu\text{m}$ Si cladding layer epitaxially grown with the same RP-CVD technique. Epitaxial growth allows the realization of low-loss fully crystalline structures while preserving IC processing compatibility.

Figure 1(a) shows a typical SEM cross-sectional image of the waveguide before and after encapsulation. The strip waveguides were 2.5-cm long [Fig. 1(b)] with widths W that varied from $0.3 \mu\text{m}$ to $2.0 \mu\text{m}$, and Ge concentrations x that varied from 0.1 to 0.3.

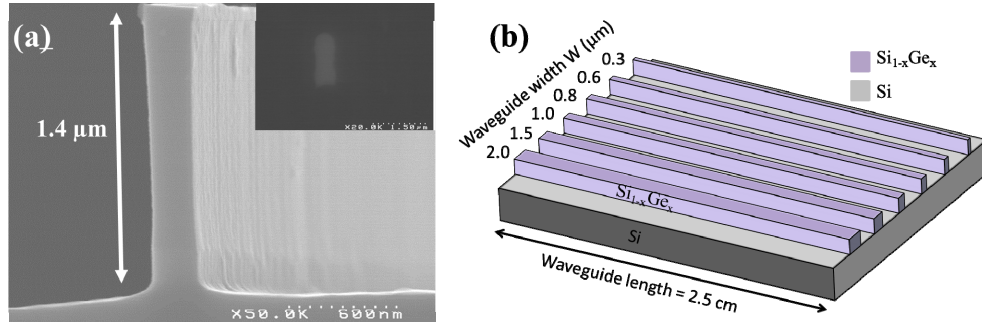


Fig. 1. (a) Scanning Electron Microscopy (SEM) image of a SiGe waveguide, before and after (inset) encapsulation. (b) Sketch of SiGe waveguides before encapsulation.

3. Waveguide design and numerical model

In order to investigate the nonlinear properties of the SiGe structures, a numerical model was developed. The model described the propagation of pump, signal and idler signals which obey the following equations [16]:

$$\frac{\partial A_p}{\partial z} = \left\{ i \left(\beta_p + \beta_p^f \right) - \frac{\alpha_p}{2} \right\} A_p + i \left(\gamma_p P_p + 2\gamma_{ps} P_s + 2\gamma_{pi} P_i \right) A_p + 2i \gamma_{pspi} A_s A_i A_p^* \quad (1)$$

$$\frac{\partial A_s}{\partial z} = \left\{ i (\beta_s + \beta_s^f) - \frac{\alpha_s}{2} \right\} A_s + i (\gamma_s P_s + 2\gamma_{sp} P_p + 2\gamma_{si} P_i) A_s + i \gamma_{sip} A_i^* A_p^2, \quad (2)$$

$$\frac{\partial A_i}{\partial z} = \left\{ i (\beta_i + \beta_i^f) - \frac{\alpha_i}{2} \right\} A_i + i (\gamma_i P_i + 2\gamma_{ip} P_p + 2\gamma_{is} P_s) A_i + i \gamma_{isp} A_s^* A_p^2, \quad (3)$$

where A_j , α_j , β_j are the electric field, linear loss and propagation constants, with $j = \{p, s, i\}$ denoting the pump, signal and idler waves respectively. The nonlinear parameter γ_{ijkl} can be calculated provided that Kerr coefficient n_2 , two photon absorption β_{TPA} , effective mode area, modal refractive index [17] and mode overlap factors are known for all possible combinations appearing in Eqs. (1)-(3) [16].

The parameters n_2 and β_{TPA} characterize the material. According to [15], Garcia's model [18] fitted to available experimental measurements, can be utilized to predict the β_{TPA} evolution of Si, Ge and $\text{Si}_{1-x}\text{Ge}_x$ alloys for all of the wavelengths of interest. The n_2 parameter can be then extracted using the nonlinear Kramers Kronig relation which links TPA values to the real part of the third order susceptibility [15]. We found that n_2 equals to 9.62×10^{-14} , 10.48×10^{-14} and $11.19 \times 10^{-14} \text{ cm}^2/\text{W}$ respectively for 10, 20 and 30% of germanium.

Some of the aforementioned quantities must be calculated for the given structure through a waveguiding analysis. By means of a Finite Elements Method (FEM) solver, the effective refractive index, the effective mode area, the confinement factor and the modal overlaps can be calculated [19]. More precisely, the effective mode area is given by:

$$A_{\text{eff}} = \frac{\left[\iint \left| \tilde{E} \right|^2 dx dy \right]^2}{\iint \left| \tilde{E} \right|^4 dx dy}, \quad (4)$$

where E governs the mode profile in the plane transverse to the propagation direction. The confinement factor is estimated from:

$$\Gamma_{xy} = \frac{\int_{-W/2}^{W/2} \int_{-H/2}^{H/2} \left| E(x, y) \right|^2 dx dy}{\iint_{xy} \left| E(x, y) \right|^2 dx dy}. \quad (5)$$

The field profile of the fundamental TM mode at 1550 nm is depicted in Fig. 2 for a waveguide with a width of 1 μm , whereas the effective mode area, the effective mode index and the confinement factor of each waveguide sample, are tabulated in Table 1.

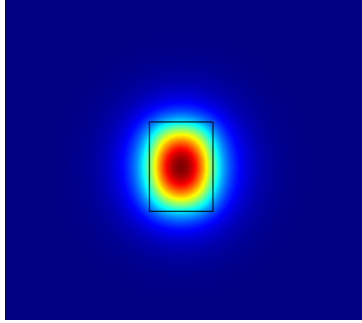


Fig. 2. Field of the TM fundamental mode for a waveguide with width 1 μm and height 1.4 μm

From the data shown in Table 1, the following can be concluded: the waveguide is predominantly quasi-TM for widths up to 1.0 μm, quasi-TE for widths above 1.5 μm and polarization insensitive at 1.5 μm (as expected due to the rectangular shape and symmetry which occurs for a $1.4 \times 1.4 \mu\text{m}^2$ profile). This can also be observed by noticing for which polarization state the effective mode area is smaller. The effective index increases with x which is natural because of the increased Ge concentration. A very interesting observation is that the effective area dramatically decreases with increasing Ge concentration which has a twofold effect. On one hand, nonlinearities are rapidly enhanced due to the smaller effective area and subsequent high energy density in the waveguide. On the other hand, as the waveguide width decreases substantially (to below 0.8 μm) the Ge core size cannot confine light effectively yielding effective areas as high as $34.24 \mu\text{m}^2$. By increasing the Ge concentration, even structures of this size can have a reasonably small effective mode area, thus allowing their usage in nonlinear processes.

Table 1. Effective mode area, effective mode index and confinement factor for all waveguides studied.

	Effective mode area (μm^2)											
	0.3 μm		0.6 μm		0.8 μm		1.0 μm		1.5 μm		2.0 μm	
	TE	TM	TE	TM	TE	TM	TE	TM	TE	TM	TE	TM
$x = 0.1$	34,24	32,09	5,49	5,31	3,95	3,87	3,45	3,41	3,33	3,34	3,65	3,68
$x = 0.2$	4,21	3,80	1,96	1,86	1,82	1,77	1,85	1,82	2,14	2,15	2,54	2,56
$x = 0.3$	2,09	1,83	1,36	1,28	1,38	1,33	1,46	1,44	1,80	1,81	2,20	2,21
	Effective mode index											
	$x = 0.1$	3,477	3,477	3,481	3,481	3,485	3,485	3,489	3,489	3,496	3,496	3,500
$x = 0.2$	3,483	3,484	3,504	3,505	3,515	3,516	3,524	3,524	3,536	3,536	3,543	3,543
$x = 0.3$	3,496	3,499	3,536	3,538	3,553	3,555	3,565	3,566	3,581	3,581	3,589	3,589
	Confinement Factor											
	$x = 0.1$	0.065	0.069	0.297	0.306	0.448	0.456	0.559	0.563	0.712	0.711	0.778
$x = 0.2$	0.199	0.22	0.558	0.57	0.692	0.7	0.772	0.78	0.863	0.86	0.897	0.894
$x = 0.3$	0.317	0.3611	0.681	0.706	0.792	0.804	0.852	0.857	0.915	0.914	0.936	0.934

The attenuation parameter (dB/cm) was extracted experimentally as it will be shown in Section 4 below, and can be safely considered to be the same for all of the pump, signal and idler waves. The parameter β_f^f which is included in Eqs. (1)-(3), represents the free-carrier induced perturbations to the propagation constant and was included in our calculations relying on Drude's model [16]. Note that, in our simulations, the free-carrier absorption (FCA) parameter was also taken into account based on Drude's model. The simulations show that its

impact on the losses experienced by the propagating waves is less important compared to the linear loss and could be comparable to that provided that the input pump exceeds 10 W of power at waveguides with $x = 0.2$. Finally, the Raman effect can be safely ignored due to its narrow bandwidth nature in silicon based waveguides [16].

The calculation of the dispersion curve is a very useful tool for the evaluation of the nonlinear properties of these waveguides. Our analysis showed that within the wavelength band under investigation, the group velocity dispersion is always normal (i.e. takes negative values) and is quite far from any zero crossing.

An interesting concept ascends when varying the Ge concentration, x . As x decreases the waveguide tends to resemble a bulk Si waveguide. Overlap between the modes at different wavelengths does not vary notably and can be safely considered to be equal to unit, since all the waves are located around 1.55 μm . However, the Ge concentration modifies the nonlinear susceptibility of the alloy and its transparency in the near-IR region. Concerning the latter, it is well known that the Si band-gap corresponds to a wavelength of 1.1 μm .

The dispersion curves for waveguide configurations with $x = 0.2$ Ge concentration and $W = 0.3, 0.6, 1.0$ and $1.5 \mu\text{m}$ width are shown in Fig. 3(a), whereas Fig. 3(b) depicts the corresponding curves for waveguides with a width $W = 1 \mu\text{m}$ for three Ge concentrations $x = 0.1, 0.2$ and 0.3 .

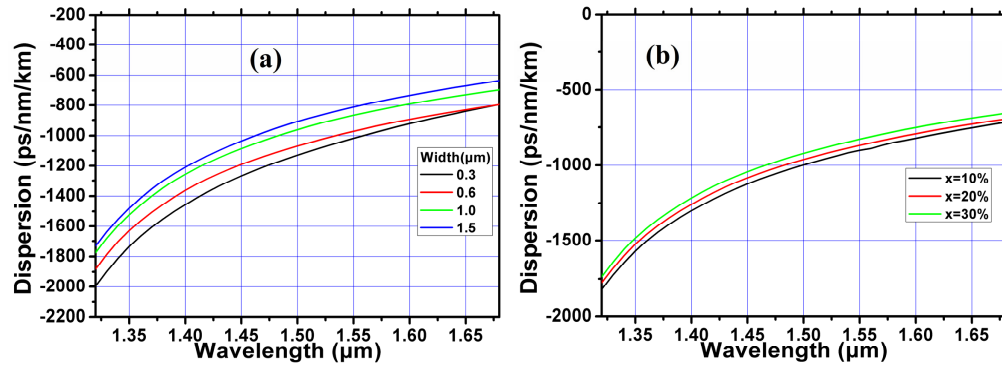


Fig. 3. Dispersion curves for (a) Ge concentration $x = 0.2$ and different waveguide width values and, (b) for width (W) equal to $1 \mu\text{m}$ and different Ge concentrations.

4. Linear loss measurement

To measure the propagation loss of the waveguides, one of the most reliable methods is based on the assessment of Fabry-Pérot (FP) resonances. If the end-faces are parallel to each other and perpendicular to the waveguide, then this waveguide acts like a FP cavity. Therefore, the transmitted power varies periodically with the optical phase difference incurred when tuning the wavelength. This method allows a measurement of the waveguide attenuation without requiring a prior knowledge of the coupling efficiency. Thus, the losses can be calculated by measuring the extinction ratio [20]:

$$\alpha L = \ln \left(R \frac{1 + \sqrt{P_{\min} / P_{\max}}}{1 - \sqrt{P_{\min} / P_{\max}}} \right), \quad (6)$$

where α is the attenuation parameter, namely the propagation loss, L is the waveguide length, P_{\min} and P_{\max} are respectively the minimum and maximum transmitted power and R is the facet reflectivity.

The experimental setup is shown in Fig. 4(a). As required by the method, the output of a continuous-wave (CW) tunable laser was coupled to the waveguide under test. The input polarization was aligned to the axes of the waveguide using a polarization controller. Then, at

the waveguide output, the light was collected by a microscope objective and directed to a power meter. A beam splitter could be placed on the optical path to direct the light to an IR camera for guided mode observation and optimization of the launching alignment. A computer-controlled routine was used to gradually sweep the laser wavelength and collect the power meter readings.

Figure 4(b) shows the measured power as a function of the wavelength for a width $W = 1 \mu\text{m}$ and for two different Ge concentrations. As expected for a FP cavity, typical fringes are observed, relating to interferences between the multiple reflections of light in the waveguide. From Eq. (6) and in agreement with the fittings, the absorption parameter α was calculated to be 0.32 cm^{-1} (1.4 dB/cm) and 1.20 cm^{-1} (5.2 dB/cm) respectively for $x = 0.2$ [Fig. 4(b1)] and $x = 0.3$ [Fig. 4(b2)].

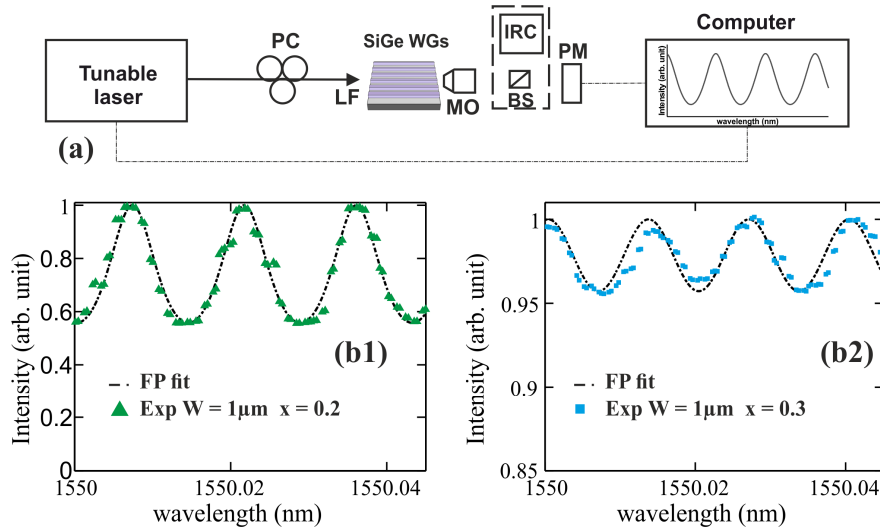


Fig. 4. (a) Experimental setup for loss measurement. PC = polarization controller, LF = Lensed Fiber, MO = Microscope Objective, BS = Beam Splitter, IRC = Infrared Camera, PM = Power meter. (b) Spectral fringes and associated FP fit for $W = 1 \mu\text{m}$ at $x = 0.2$ (b1), and at $x = 0.3$ (b2).

We carried out systematic measurements of the losses for the whole set of the available waveguides. The results are reported in Table 2 as a function of the width and the Ge concentration. When these results are compared with the confinement factor [Eq. (5)] and effective mode area [Eq. (4)] calculations of Table 1, a clear correlation is drawn. With decreasing waveguide width losses increase due to poor confinement. On the other hand, with increasing width the confinement factor rapidly increases which results in higher overlap of the mode and the lossier SiGe core. This can also be confirmed by the fact that for the same Ge concentration losses increase as the confinement factor increases. This means that there is an optimal value for low losses at each concentration although this is not clearly shown in the $x = 0.3$ case probably due to uncertainty in the measurements estimated to be close to 10%.

Moreover, as expected, for a fixed waveguide width, the Germanium strongly increases the absorption loss. For instance, at $W = 1.5 \mu\text{m}$, the losses evolve from 0.43 to 4.77 dB/cm when Ge concentration increases from 0.1 to 0.3 . Note that low concentration ($x = 0.1$) leads to high loss when the width is too small ($\leq 1.0 \mu\text{m}$) because of the poor confinement of light into the small-dimension waveguide, as was also reported in Section 3. We believe that the poor confinement together with the high coupling losses have likely led to larger experimental errors in our measurements for the $x = 0.1$ concentration samples relative to the higher Ge concentrations, as will also be seen below (section 5.2). Note also that the propagation losses are very similar for the TE and TM modes.

Table 2. Loss in dB/cm for the SiGe waveguides depending on width and concentration in Ge.

	x = 0.1	x = 0.2	x = 0.3
0.3 μm	High loss (> 5 dB/cm)	3.90	3.47
0.6 μm		2.38	4.56
0.8 μm		2.38	4.77
1.0 μm	4.75	1.40	5.21
1.5 μm	0.43	1.52	4.77
2.0 μm	0.65	2.60	4.34

5. Nonlinearity

5.1 Two-photon absorption

Two-Photon Absorption (TPA) refers to a transition from the ground state of a system to a higher energy state through the absorption of two photons. This nonlinear absorption is detrimental by limiting the maximum transmitted power. The TPA coefficient, noted here β_{TPA} , is related to the ratio of input power P_{in} to output power P_{out} as follows [21, 22]:

$$\frac{P_{in}}{P_{out}} = \frac{1}{T} = \exp(\alpha L) \frac{\beta_{TPA} L_{eff} P_{in}}{A_{eff}} + \exp(\alpha L). \quad (7)$$

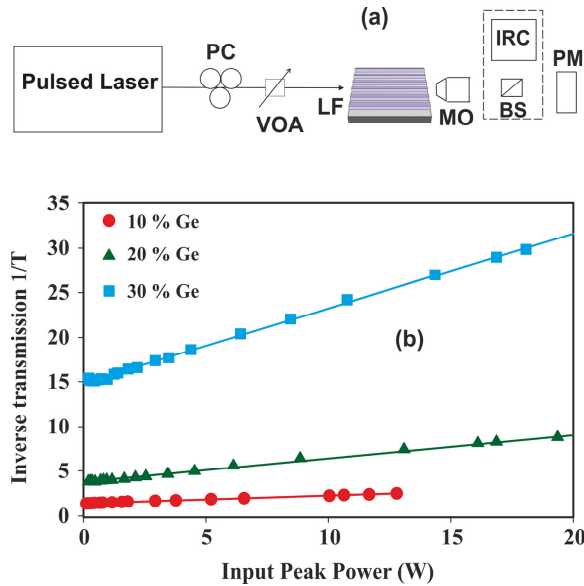


Fig. 5. (a) Experimental setup for the TPA measurement. VOA = variable optical attenuator (b) Inverse transmission versus coupled input peak power for x = 0.1 (red circles), x = 0.2 (green triangle) and x = 0.3 (blue square). The solid lines correspond to a linear fit.

Figure 5(a) shows the experimental setup for the TPA coefficient measurement. A pulsed source centered at 1550 nm producing 0.5 ps optical pulses with a 20-MHz repetition rate was used. A variable attenuator with an integrated power monitor controlled the input power. Note that the effects of free-carrier absorption were neglected. Figure 5(b) presents the inverse transmission corresponding to the ratio of input power to output power as a function of the input peak power for the three different concentrations in Germanium (here $W = 2.0 \mu\text{m}$). As expected from Eq. (7), the TPA value can be extracted by applying a linear fit to this measurement, and making use of the previously measured values of loss and nonlinearity.

Note that from the y-intersect we recover the linear loss. The TPA values are reported in Table 3 and compared to the theoretical values. A clear increase in the TPA is observed when the germanium concentration increases [15]. Even though the trend predicted from both the experimental and theoretical values is similar, a discrepancy is observed. We consider the main reason for this discrepancy to be an overestimation of the theoretical value for the silicon TPA. In our theoretical model, this was calculated following Garcia's model, fitting on the measurements of Bristow *et al.* in [23]. It is noted that even in the same reference, a comparison of the model with experimental results also suggests an overestimation of the TPA value. Although there is a discrepancy between measured and theoretically calculated TPA values, the numerically predicted n_2 values estimated using the Kramers-Kronig nonlinear relation are pretty close to the real ones as proven by the experimental characterization of the FWM efficiency of the devices shown in section 6. This can be understood since the power levels used in all of our characterization experiments (apart from those presented in Fig. 5) were too low for TPA to have any significant impact.

Table 3. TPA values in cm/GW for the SiGe waveguides depending on concentration in Ge.

Ge concentration	Experimental β_{TPA} (cm/GW)	Theoretical β_{TPA} (cm/GW)
x = 0.1	1.16	1.73
x = 0.2	1.24	2.15
x = 0.3	1.5	2.58

5.2 Nonlinear parameter γ

To measure the nonlinearity, a method based on the measurement of the nonlinear phase shift of a dual-frequency beat signal was utilized [24]. Indeed, a beat signal undergoes a nonlinear phase shift given by:

$$\varphi_{\text{SPM}} = 2\gamma L_{\text{eff}} P, \quad (8)$$

where γ and L_{eff} are respectively the nonlinear coefficient, defined as $\gamma = 2\pi n_2 / (\lambda A_{\text{eff}})$, and the effective length of the waveguide under test and P is the average power of the signal. The nonlinear phase shift is related to the conversion efficiency (CE) as:

$$[CE_{\text{linear}}]^{-1} = \frac{J_0^2(\varphi_{\text{SPM}}/2) + J_1^2(\varphi_{\text{SPM}}/2)}{J_1^2(\varphi_{\text{SPM}}/2) + J_2^2(\varphi_{\text{SPM}}/2)}, \quad (9)$$

where J_i is the Bessel function of the i -th order.

For this measurement, we used the setup shown in Fig. 6(a), where two CW signals were coupled into the waveguide under test after amplification and polarization control. The two wavelengths were chosen sufficiently close to avoid the onset of dispersive effects [25]. The polarization was adjusted such that the nonlinear response was maximized when analyzed using an OSA at the output.

By measuring spectrally the conversion efficiency [Fig. 6(b)] and using Eq. (9), we plotted the nonlinear phase shift as a function of the average power as shown in Fig. 6(c) for two different Ge concentrations of the 1 μm -width waveguide. The nonlinear parameter γ was then obtained from the slope of the linear function [Eq. (8)] which fitted the experimental data.

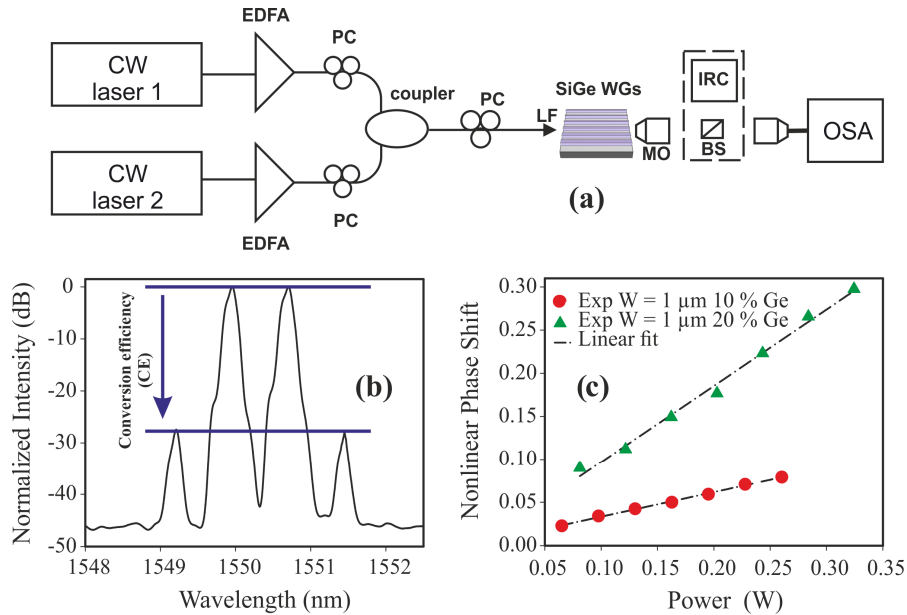


Fig. 6. (a) Experimental setup for nonlinearity measurement. EDFA = Erbium Doped Fiber Amplifier, OSA = Optical Spectrum Analyzer. (b) Typical spectrum where the conversion efficiency can be read (c) Typical plots of the Nonlinear Phase shift vs. the signal power for $W = 1 \mu\text{m}$ and either $x = 0.1$ (red circles) or $x = 0.2$ (green triangles). The dotted-dashed lines correspond to linear fits.

All results are summarized in Fig. 7. As expected from the literature [15], the nonlinearity increases with the Ge concentration. Smaller waveguide widths also result in higher values of γ , up to a value where the mode can no longer be confined in a small area, and the trend is reversed. Typically, the maximum value is reached for widths between $0.8 \mu\text{m}$ and $1.0 \mu\text{m}$. These results were also compared with simulations and the results are contrasted in Fig. 7.

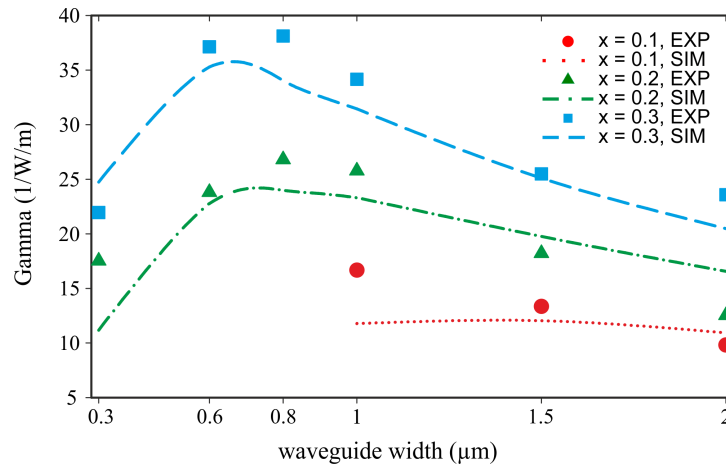


Fig. 7. Nonlinear parameter γ as a function of the waveguide width for $x = 0.1$ (red circles), 0.2 (green triangles) and 0.3 (blue squares). The experimental results (symbols) are compared with numerical simulations in dotted ($x = 0.1$), dotted-dashed ($x = 0.2$) and dashed ($x = 0.3$) lines.

6. Dispersion and conversion efficiency

Although it would be possible to measure the dispersion curve experimentally using a Mach-Zehnder interferometer [4, 26, 27], we have focused our attention on the impact of dispersive

effects on the FWM-induced conversion efficiency. The calculations of Section 3 have suggested that the telecommunications C-band is far from the zero-dispersion wavelength of the SiGe waveguides included in our study, and it is well known that the dispersion could drastically impact on the four-wave mixing bandwidth [28, 29]. In order to assess the impact of the dispersion and also to validate the previous simulations on dispersion (as presented in Fig. 3), we have experimentally measured the conversion efficiency as a function of wavelength.

The experimental setup is similar to Fig. 6(a) where “laser 1” is the pump having a fixed wavelength centered at 1550 nm and “laser 2” is a tunable continuous wave signal with low power compared to the pump. We report in Fig. 8 the wavelength dependence of the FWM conversion efficiency for the best of the waveguides (see the following Section and Fig. 9) for each Ge concentration. The simulations, which were derived by solving the three coupled nonlinear equations for the pump, signal and idler, are in relatively good agreement with the experimental data, thus confirming the validity of the dispersion curves of Fig. 3.

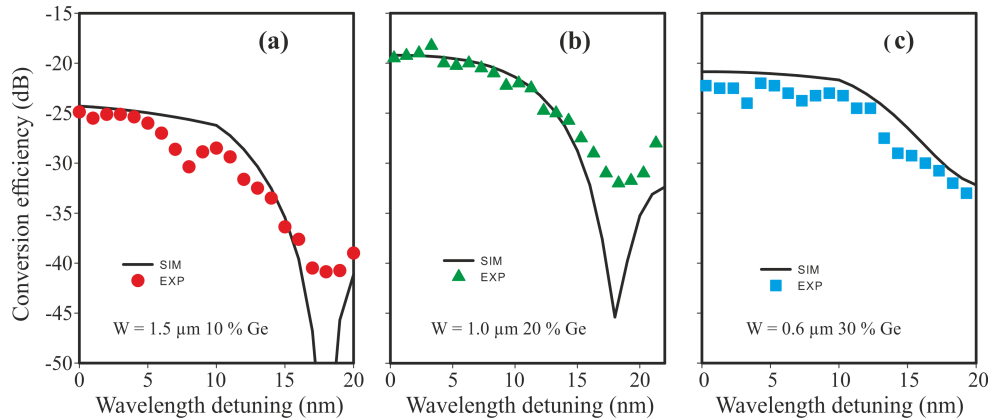


Fig. 8. Conversion efficiency as a function of wavelength detuning from 1550 nm for (a) $W = 1.5 \mu\text{m}$ and $x = 0.1$ (red circles) (b) $W = 1.0 \mu\text{m}$ and $x = 0.2$ (green triangles) and (c) $W = 0.6 \mu\text{m}$ and $x = 0.3$ (blue squares). The solid lines correspond to numerical simulations. The input power was close to 295 mW.

Moreover, for a total power of $\sim 295\text{mW}$ at the input of the waveguide, the Fig. 8 shows a 3dB bandwidth of $\sim 19 \text{ nm}$ [Fig. 8(a)], $\sim 21 \text{ nm}$ [Fig. 8(b)] and $\sim 26 \text{ nm}$ [Fig. 8(c)] respectively for $x = 0.1$, $x = 0.2$ and $x = 0.3$. Note also that from our full set of measurements (not shown here), it was observed that, for a given waveguide width, a higher Germanium concentration results in a broader FWM bandwidth. The results emphasize that the inclusion of Ge in the alloys allows an additional degree of freedom in the design of the optical properties of nonlinear waveguides.

7. Discussion on performance

Even though these SiGe waveguides were not specifically designed and optimized for nonlinear applications, the previous section has shown that their performance as broadband FWM-based devices operating in the C-band is noteworthy.

A common way to assess the performance of waveguides is the two-photon absorption figure of merit defined as $\text{FOM}_{\text{TPA}} = n_2 / (\beta_{\text{TPA}} \lambda)$ [30]. For the SiGe waveguides we considered in this study, this figure of merit takes values ranging from 0.55 to 0.48 as the Ge concentration increases from 10% to 30%. These values are close to the silicon FOM_{TPA} (typically 0.38 ± 0.17 [30]) indicating that SiGe has the potential to be a competitive waveguide technology. This TPA figure of merit is mainly used to assess whether TPA is a limiting factor when a material is considered for use in all-optical switching [31, 32]. However, for the amounts of coupled power considered in these experiments ($\leq 300 \text{ mW}$), the impact of TPA was not strongly significant (see Fig. 5). Therefore, for a fairer assessment of

the relative performance of the waveguides with respect to their linear loss and nonlinearity, one can use a simpler figure of merit, defined here as $FOM = \gamma L_{\text{eff}}$. Figure 9 is a plot of the FOM for each of the waveguides we characterised. Clearly, the best performance is reached for $x = 0.2$ and $W = 1.0 \mu\text{m}$.

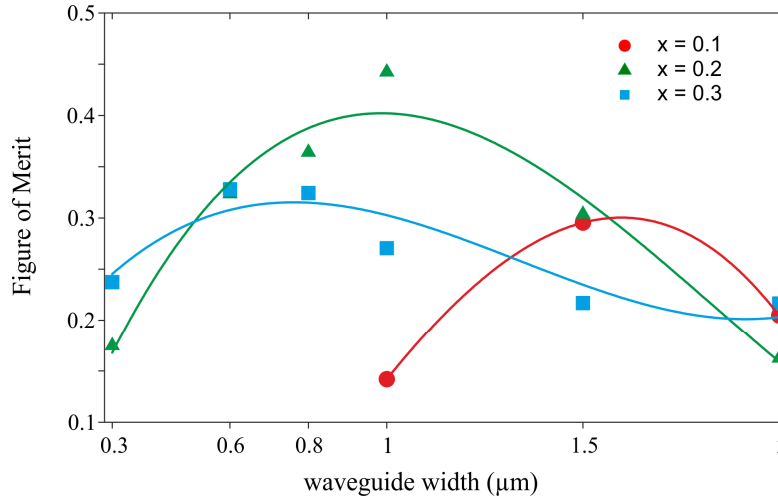


Fig. 9. Figure of Merit as a function of the waveguide width for $x = 0.1$ (red circles), 0.2 (green triangles) and 0.3 (blue squares). The solid lines, corresponding to cubic polynomial fits, are only to guide the eye.

Due to the fact that the losses are not significantly dependent on the polarization and that the effective area is also very similar for TE and TM modes, the performance is not strongly affected by the polarization.

Note that one could anticipate attaining much higher FOMs through adopting a more complex waveguide design. Indeed, as for the silicon [6, 30], both the waveguide nonlinearity and dispersion properties at 1550 nm can be significantly improved after appropriate engineering, thus making this waveguide technology a potential competitor to other state-of-art nonlinear waveguides with a new degree of freedom, namely, the germanium concentration profile.

8. Conclusion

We have reported a systematic study on the linear and nonlinear optical properties of SiGe waveguides at telecommunication wavelengths. We have confirmed that Germanium increases the nonlinearity but also the linear and nonlinear loss compared to pure silicon. Depending on the width, the nonlinear parameter γ may exceed $30 \text{ W}^{-1} \cdot \text{m}^{-1}$. Efficient FWM can be produced while retaining pump power levels well below the onset of TPA. We have explored the tradeoffs between loss and nonlinearity for different waveguide designs and Ge concentrations.

This study confirms that $\text{Si}_{1-x}\text{Ge}_x$ is a promising candidate not just for the mid-infrared but also for all-optical processing at telecommunication wavelengths [33, 34]. The findings of this paper can inform the design of optimized nonlinear waveguides, allowing the manipulation of not just the waveguide dimensions but also the material composition.

Acknowledgments

This work was supported by the European Communities Seventh Frame-work Programme FP7/2007-2013 under Grant 288304 (STREP CLARITY).